Optimization Method for the Energy and Emissions Management of a Hybrid Electric Vehicle with an Exhaust Aftertreatment System

Author(s):
Ritzmann, Johannes; Lins, Georg; Onder, Christopher

Publication date:
2020-11

Permanent link:
https://doi.org/10.3929/ethz-b-000460632

Originally published in:
IFAC-PapersOnLine 53(2), https://doi.org/10.1016/j.ifacol.2020.12.888

Optimization Method for the Energy and Emissions Management of a Hybrid Electric Vehicle with an Exhaust Aftertreatment System

J. Ritzmann *, **G. Lins** *, **C. Onder** *

* *Institute for Dynamic Systems and Control, ETH Zurich, 8092 Zurich, Switzerland*

Abstract: This paper presents a real-time optimization method to compute the fuel-optimal torque split, gear selection and engine on/off command for a Diesel hybrid electric vehicle equipped with an exhaust aftertreatment system. We aim to minimize the amount of fuel consumed, while achieving a charge-sustaining operation and keeping the tailpipe NO_x emissions below the legislative limit. We simplify the full vehicle model to facilitate the formulation of a mixed-integer convex problem which is then solved using the proposed iterative convex optimization (ICO) algorithm. We validate the result by comparing it to the globally optimal solution computed using dynamic programming (DP). For the simple model, the ICO algorithm finds the same solution as the DP benchmark. The computation time was reduced from one week for the DP benchmark to 49 s for the ICO solution. By comparing the DP solution obtained on the full model with the ICO solution evaluated on the full model, we observe an offset in the solution due to model mismatch, but find that the ICO algorithm captures the qualitative trends of the optimal solution. The proposed algorithm is capable of solving the energy and emissions management problem in real-time, forming the basis for online optimal control.

Keywords: hybrid electric vehicle, energy and emissions management, aftertreatment system, optimal control, mixed-integer optimization

1. INTRODUCTION

To exploit the full potential for a reduction of the fuel consumption and the emissions of a hybrid electric vehicle (HEV), the available degrees of freedom need to be carefully controlled. In parallel-hybrid vehicles, these are the torque split between the electric motor and the internal combustion engine, the selected gear, and the engine on/off command. Today's Diesel-powered vehicles are equipped with an exhaust gas aftertreatment system (ATS) to reduce the NO_x emissions and care must be taken to guarantee a sufficient ATS temperature for the chemical reactions to occur. The full system performance can only be achieved if the resulting optimal control problem (OCP) is solved for the current vehicle mission and an online optimal controller which can exploit predictive information about the driving mission is used, e.g., a model predictive control (MPC) scheme. Both the battery state of charge and the ATS temperature must be considered in a dynamic optimization. Thereby, the goal is to minimize the amount of fuel consumed, while achieving a charge-sustaining operation and keeping the tailpipe NO_x emissions below the legislative limit. As both continuous inputs and discrete inputs need to be considered, a mixed-integer OCP results. A problem of this class is very challenging to solve (Lee and Leyffer (2011)). Furthermore, this OCP must be solved online using the limited computing power aboard an HEV, requiring an extremely efficient optimization method. In this paper we propose an algorithm to rapidly solve this optimization problem.

The classical energy management problem for HEVs has been in the focus of extensive research throughout the last decades. A summary of typical approaches is presented in Sciarretta and Guzzella (2007). If the dependency of the Hamiltonian on the battery state of charge is neglected, Pontryagin's Minimum Principle (PMP, Boltyanski et al. (1960)) can be used to simplify the problem to finding a constant equivalence factor that characterizes the trade-off between fuel energy and battery energy. If predictive data is available, a reference trajectory for the state of charge can be calculated. The equivalent consumption minimization strategy is often used, where the optimal control inputs are calculated based on the equivalence factor which is set by a feedback controller in order to follow a state-of-charge reference. An example is given in Ambühl (2009). Classical energy management methods for HEVs do not consider pollutant emissions and therefore cannot guarantee that the vehicle is operated within the legislative emission limit.

In some publications, the engine-out NO_x emissions of the internal combustion engine are considered in the OCP, but the ATS temperature and its capability to reduce the NO_x emissions are not taken into account. Using PMP, the authors of Zentner et al. (2014) show that a second equivalence factor can be introduced which characterizes the trade-off between fuel energy and NO_x

emissions. In Nüesch et al. (2014a), this result is used to develop an equivalent energy and emissions strategy that controls both the equivalence factor corresponding to the electrical energy consumption and the one corresponding to the engine-out emissions. In the form presented, that approach does not control the optimal discrete inputs but sets them using a heuristic method. To guarantee emissions compliance for a vehicle equipped with an ATS, that method is not sufficient, as it does not consider the influence of the ATS on the tailpipe emissions.

If the ATS is taken into account in the OCP, an approach such as the one presented in Kessels et al. (2010) can be used to show that the costate, aka the equivalence factor, corresponding to the ATS temperature, is not constant and that the previously introduced equivalent energy and emissions strategy control methods no longer work reliably. Several publications, such as Tschopp et al. (2015) or Simon et al. (2018), solve the resulting OCP offline using dynamic programming (DP, Bellman (1956)). The authors state that about one week is required to solve the OCP, rendering the optimization method unsuitable for online control.

Only a limited number of real-time optimal energy and emissions management controllers for HEVs could be found in literature. The method presented in Kessels et al. (2010) is applied to a series-hybrid vehicle and considers the NO_x reduction effect of the ATS, but neglects the effect of the chosen strategy on the ATS temperature. Furthermore, the publication does not state clearly whether the engine can be switched off, and it does not consider any predictive information. In Kuchly et al. (2019), MPC is applied to a mild parallel hybrid. The OCP is solved using a projected gradient method and considers predictive information for a horizon of 10 s. Discrete inputs are not included in the optimization. A further MPC approach is presented in Zhao and Wang (2014) where the optimization method used to solve the OCP is not stated and where the text is unclear as to whether discrete inputs were considered. In Ma and Wang (2017), a method is presented that finds the optimal control parameters for a predefined controller structure in an MPC fashion, thereby sacrificing a significant portion of the available system performance. No real-time optimization method capable of solving the mixed-integer energy and emissions management problem for HEVs could be found in literature.

This paper presents a real-time optimization method to solve the mixed-integer energy and emissions management problem. Specifically, we first present the HEV powertrain architecture considered and its mathematical model. Second, we simplify the HEV model to facilitate the formulation of a mixed-integer convex problem (MICP). Third, the iterative convex optimization (ICO) algorithm to solve the resulting MICP is outlined. Fourth, the performance of the ICO algorithm is compared to a DP benchmark. Finally, the advantages of the proposed method are summarized and the areas for further improvement are identified.

2. HEV POWERTRAIN

Figure 1 shows the parallel-hybrid powertrain considered in this work. It features a single electric machine connected to the torque splitter via a fixed-transmission-ratio gearbox and drawing power from the battery via a DC-DC converter. The Diesel engine is connected to the torque splitter via a clutch and a six-speed automatic gearbox and it features an ATS consisting of a Diesel oxidation catalyst (DOC), a Diesel Particulate filter (DPF), and a selective catalytic reduction (SCR) system. The degrees of freedom that have to be set by the energy and emissions management system are the clutch position (engaged/disengaged), the selected gear of the engine gearbox, and the torque split. The clutch position and the selected gear are combined in the discrete variable i_{gb}, where $i_{\mathrm{gb}} = 0$ represents a disengaged clutch, i.e., engine off, and $i_{\mathrm{gb}} > 0$ represents an engaged clutch, i.e., engine on, with the gear $i_{\mathrm{gb}} \in \{1, 2, 3, 4, 5, 6\}$ selected. The torque split is set by the continuous input P which represents the electric motor power at the torque splitter.

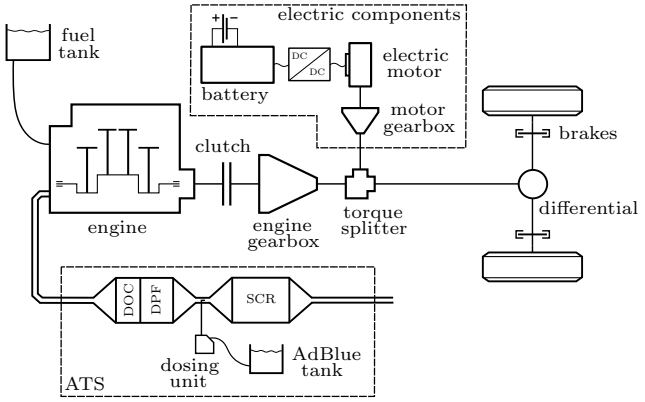

Fig. 1. Parallel-hybrid powertrain with ATS.

Only the most important relations and the sub-models regarding emissions are presented in the following, as the powertrain model without the emissions considerations was already presented in Ritzmann et al. (2019).

2.1 Vehicle Dynamics

The rotational speed and the traction power at the torque splitter are calculated from the vehicle dynamics and the driving mission as

$$\omega_{\mathrm{ts}} = \frac{\gamma_{\mathrm{fd}}}{r_{\mathrm{w}}} \cdot v \tag{1}$$

$$P_{\mathrm{ts}} = v \cdot \Big(F_{\mathrm{d}}(\Gamma, v) + F_{\mathrm{m}}(a) \Big) , \tag{2}$$

where r_{w} is the wheel radius, γ_{fd} is the final drive ratio, Γ is the road gradient, v is the vehicle velocity, a is the vehicle acceleration, F_{d} is the drag force, i.e. aerodynamic drag, rolling resistance and gravitational force, and F_{m} is the inertial force.

The friction brakes are only used when the engine is switched off. The braking power P_{br} cannot be larger than zero.

$$P_{\mathrm{br}} = \begin{cases} P_{\mathrm{ts}} - P & \text{if } i_{\mathrm{gb}} = 0 \\ 0 & \text{if } i_{\mathrm{gb}} > 0 \end{cases} \tag{3}$$

2.2 Electrical Components

The motor gearbox and the DC-DC converter are modelled using a constant efficiency. The motor efficiency is given

as a map of the motor speed and torque. The battery is modelled using an equivalent circuit model, where both the open-circuit voltage V_{oc} and the internal resistance R_{int} depend on the battery state of charge. The state-of-charge dynamics are

$$\frac{\mathrm{d}\xi}{\mathrm{d}t} = -\frac{P_{\mathrm{b}}(P,\xi)}{Q_{\max} V_{\mathrm{oc}}(\xi)}\,, \tag{4}$$

where ξ is the state of charge, P_{b} is the power drawn from the battery, and $Q_{\max}$ is the maximum capacity of the battery. The limit on the motor torque $T_{\mathrm{m}} \in [T_{\mathrm{m,min}}(\omega_{\mathrm{m}}),\ T_{\mathrm{m,max}}(\omega_{\mathrm{m}})]$ and the limit on the battery current $I_{\mathrm{b}} \in [I_{\mathrm{b,min}},\ I_{\mathrm{b,max}}]$ are summarized in the limit for the motor power at the torque splitter, resulting in $P \in [P_{\min}(\omega_{\mathrm{m}},\xi),\ P_{\max}(\omega_{\mathrm{m}},\xi)]$. The dependency on ξ results from the battery losses that depend on the state of charge. The motor speed limit is given by $\omega_{\mathrm{m}} \in [0, \omega_{\mathrm{m,max}}]$. The battery state of charge is limited to $\xi \in [\xi_{\min},\ \xi_{\max}]$.

2.3 Engine

Given P, the engine power at the torque splitter is

$$P_{\mathrm{e,ts}} = P_{\mathrm{ts}} - P - P_{\mathrm{br}}\,. \tag{5}$$

The engine speed is set by ω_{ts}, and i_{gb}, whereas the engine torque is set by $P_{\mathrm{e,ts}}$, i_{gb}, and the efficiency of the engine gearbox. The fuel power P_{f}, the engine-out $\mathrm{NO_x}$ mass flow $\overset{*}{m}{}^{\mathrm{eo}}_{\mathrm{NO_x}}$, the exhaust temperature ϑ_{exh}, and the exhaust mass flow $\overset{*}{m}_{\mathrm{exh}}$ are related to the engine speed and torque through static maps. The limit of the engine power at the torque splitter is $P_{\mathrm{e,ts}} \in [0,\ P_{\mathrm{e,ts,max}}(\omega_{\mathrm{e}})]$. The engine speed limit is $\omega_{\mathrm{e}} \in [\omega_{\mathrm{e,min}},\ \omega_{\mathrm{e,max}}]$ if the engine is on and $\omega_{\mathrm{e}} = 0$ if it is off.

2.4 Aftertreatment System

In this work, we focus on $\mathrm{NO_x}$ emissions and disregard all other emission species. Both the DOC and the DPF bricks have a catalytic coating to promote the oxidation of NO. The SCR catalyst is used to reduce the $\mathrm{NO_x}$ emissions. To facilitate the optimization, a very simple model of the ATS is required.

We capture the thermal behaviour of the ATS using a single-cell 0D first-principle model, where the mass of the ATS m_{ATS} and the convective heat transfer coefficient α_{hl} are parameters fitted to measurement data. The dynamics of the ATS temperature are

$$\frac{\mathrm{d}\vartheta_{\mathrm{ATS}}}{\mathrm{d}t} = \frac{1}{m_{\mathrm{ATS}} c_{\mathrm{ATS}}} \cdot (\overset{*}{H}_{\mathrm{ATS}} - \overset{*}{Q}_{\mathrm{hl}}) \tag{6}$$

$$\overset{*}{H}_{\mathrm{ATS}} = \overset{*}{m}_{\mathrm{exh}} c_{\mathrm{p}} \cdot (\vartheta_{\mathrm{exh}} - \vartheta_{\mathrm{ATS}}) \tag{7}$$

$$\overset{*}{Q}_{\mathrm{hl}} = \alpha_{\mathrm{hl}} S \cdot (\vartheta_{\mathrm{ATS}} - \vartheta_{\mathrm{amb}})\,, \tag{8}$$

where c_{ATS} is the specific heat capacity of the ATS. The enthalpy flow from the exhaust gas to the ATS is denoted by $\overset{*}{H}_{\mathrm{ATS}}$, where c_{p} is the specific heat capacity at constant pressure of the exhaust gas, ϑ_{exh} is the exhaust gas temperature, and ϑ_{ATS} is the ATS temperature. The conductive heat loss to the environment is denoted by $\overset{*}{Q}_{\mathrm{hl}}$, where S is the outer surface area of the ATS and ϑ_{amb} is the ambient temperature.

For the chemical model of the ATS, we use a static look-up map which gives the $\mathrm{NO_x}$-reduction efficiency η_{DeNOx} as a function of the ATS temperature and the exhaust mass flow. This map incorporates the effects of the DOC, the DPF, and the SCR. It is obtained using steady-state evaluations of a more sophisticated ATS model developed based on Käfer (2004). The dynamics of the accumulated tailpipe $\mathrm{NO_x}$ mass are

$$\frac{\mathrm{d}m^{\mathrm{tp}}_{\mathrm{NO_x}}}{\mathrm{d}t} = \Big(1 - \eta_{\mathrm{DeNOx}}(\vartheta_{\mathrm{ATS}}, \overset{*}{m}_{\mathrm{exh}})\Big) \cdot \overset{*}{m}{}^{\mathrm{eo}}_{\mathrm{NO_x}}\,. \tag{9}$$

3. OPTIMAL CONTROL PROBLEM

The HEV powertrain model used in this work is defined by the input vector $\underline{u}$ and the state vector $\underline{x}$.

$$\underline{u} = \begin{bmatrix} P \\ i_{\mathrm{gb}} \end{bmatrix} \qquad \underline{x} = \begin{bmatrix} \xi \\ \vartheta_{\mathrm{ATS}} \\ m^{\mathrm{tp}}_{\mathrm{NO_x}} \end{bmatrix} \tag{10}$$

The resulting OCP is

$$\underset{P,\, i_{\mathrm{gb}}}{\text{minimize}} \quad \int_0^{t_{\mathrm{fin}}} P_{\mathrm{f}}\,\mathrm{d}t \tag{11a}$$

subject to

$$\text{Eqs. (1)} - \text{(9)} \tag{11b}$$
$$\xi(0) = \xi_0 \tag{11c}$$
$$\xi(t_{\mathrm{fin}}) \geq \xi_0 \tag{11d}$$
$$\xi \in [\xi_{\min},\ \xi_{\max}] \tag{11e}$$
$$\vartheta_{\mathrm{ATS}}(0) = \vartheta_{\mathrm{ATS},0} \tag{11f}$$
$$m^{\mathrm{tp}}_{\mathrm{NO_x}}(0) = 0 \tag{11g}$$
$$m^{\mathrm{tp}}_{\mathrm{NO_x}}(t_{\mathrm{fin}}) \leq \overline{m}^{\mathrm{tp}}_{\mathrm{NO_x}} \tag{11h}$$
$$P_{\mathrm{br}} \leq 0 \tag{11i}$$
$$\omega_{\mathrm{m}} \in [0,\ \omega_{\mathrm{m,max}}] \tag{11j}$$
$$P \in [P_{\min}(\omega_{\mathrm{m}},\xi),\ P_{\max}(\omega_{\mathrm{m}},\xi)] \tag{11k}$$
$$\omega_{\mathrm{e}} \in \begin{cases} \{0\} & \text{if } i_{\mathrm{gb}} = 0 \\ [\omega_{\mathrm{e,min}},\ \omega_{\mathrm{e,max}}] & \text{if } i_{\mathrm{gb}} > 0 \end{cases} \tag{11l}$$
$$P_{\mathrm{e,ts}} \in [0,\ P_{\mathrm{e,ts,max}}(\omega_{\mathrm{e}})] \tag{11m}$$
$$i_{\mathrm{gb}} \in \{0,1,2,3,4,5,6\}\,. \tag{11n}$$

The initial state of charge is ξ_0, the initial ATS temperature is $\vartheta_{\mathrm{ATS},0}$, and the limit on the accumulated tailpipe $\mathrm{NO_x}$ mass is $\overline{m}^{\mathrm{tp}}_{\mathrm{NO_x}}$. The final time is denoted by t_{fin}.

As a benchmark for the optimization method developed in this work, this OCP is solved using DP. We use the function `dpm` presented in Sundström and Guzzella (2009). Solving the OCP with DP takes about one week for a driving mission with a duration of 20 minutes and a discretization of 1 s.

4. FORMULATION OF MICP

In this section we simplify the HEV model to facilitate the reformulation of the OCP given by (11) as a mixed-integer convex problem (MICP).

4.1 Model Simplifications

As presented in Ritzmann et al. (2019), a piecewise quadratic approximation is used to model the battery

power P_b and the fuel power P_f. The dependency of P_b on the state of charge is neglected.

$$P_\mathrm{b} = \begin{cases} \alpha P^2 + \beta_1 P & \text{if } P \geq 0 \\ \alpha P^2 + \beta_2 P & \text{if } P < 0 \end{cases} \tag{12}$$

$$P_\mathrm{f} = \begin{cases} 0 & \text{if } i_\mathrm{gb} = 0 \\ \kappa_2 P_\mathrm{e,ts}^2 + \kappa_1 P_\mathrm{e,ts} + \kappa_0 & \text{if } i_\mathrm{gb} > 0 \end{cases} \tag{13}$$

The coefficients α and β of the electrical component model are dependent on the motor speed ω_m, while the coefficients κ of the engine model are dependent on the engine speed ω_e.

The enthalpy flow from the exhaust gas to the ATS and the engine-out $\mathrm{NO_x}$ emissions are modelled as

$$\overset{*}{H}_\mathrm{ATS} = \begin{cases} 0 & \text{if } i_\mathrm{gb} = 0 \\ \delta_2 \vartheta_\mathrm{ATS} + \delta_1 \cdot (P_\mathrm{f} - P_\mathrm{e,ts}) + \delta_0 & \text{if } i_\mathrm{gb} > 0 \end{cases} \tag{14}$$

$$\overset{*}{m}{}^\mathrm{eo}_\mathrm{NOx} = \nu_2 P_\mathrm{f}^2 + \nu_1 P_\mathrm{f} \,, \tag{15}$$

with coefficients δ and ν that depend on the engine speed ω_e. Equation (7) of the ATS thermal model is approximated by (14), while (6) and (8) remain unchanged.

The form of the static map for the chemical ATS model from Eq. (9) is adapted in order to facilitate the formulation of a MICP. By assuming a fixed ratio between $\overset{*}{m}{}^\mathrm{eo}_{\mathrm{NO_x}}$ and $\overset{*}{m}_\mathrm{exh}$, we neglect the explicit dependency of $\overset{*}{m}{}^\mathrm{tp}_{\mathrm{NO_x}}$ on the $\mathrm{NO_x}$ concentration in the exhaust gas. The adapted map gives the tailpipe $\mathrm{NO_x}$ mass flow as a function of the ATS temperature and the engine-out $\mathrm{NO_x}$ mass flow as shown in Fig 2.

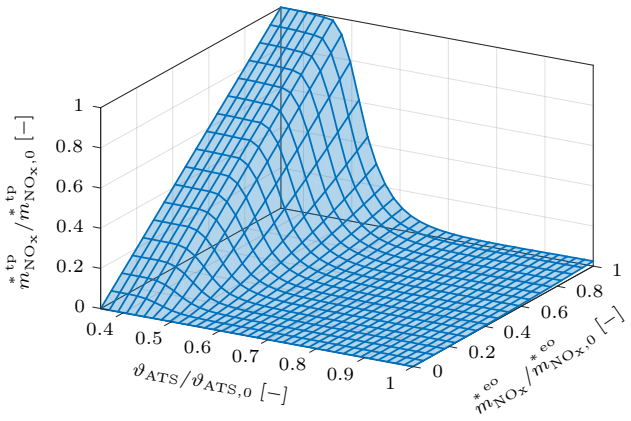

Fig. 2. Adapted static look-up map for the chemical ATS model. All values are normalized.

The map in Fig. 2 clearly is not convex. In order to nevertheless allow a region-wise convex approximation, the map is split into two regions at the threshold temperature $\vartheta_\mathrm{ATS,thr}$. For $\vartheta_\mathrm{ATS} < \vartheta_\mathrm{ATS,thr}$, no $\mathrm{NO_x}$ reduction takes place. This region is denoted by the ATS binary value $b_\mathrm{ATS} = 0$. For $\vartheta_\mathrm{ATS} \geq \vartheta_\mathrm{ATS,thr}$, $\mathrm{NO_x}$ reduction takes place. This region is denoted by the ATS binary value $b_\mathrm{ATS} = 1$ and is further split into four sub-regions depending on the engine-out $\mathrm{NO_x}$ mass flow. These sub-regions are denoted by the ATS integer $i_\mathrm{ATS} \in \{0, 1, 2, 3\}$. Each sub-region of the ATS map is approximated using a set of linear functions that form a convex epigraph when relaxed. Each linear function has the form

$$\overset{*}{m}{}^\mathrm{tp}_\mathrm{NOx} = \tau_2 \vartheta_\mathrm{ATS} + \tau_1 \overset{*}{m}{}^\mathrm{eo}_\mathrm{NOx} + \tau_0 \,. \tag{16}$$

The coefficients τ_2, τ_1, and τ_0 for each linear function of the set are summarized in the vectors $\underline{T}_2$, $\underline{T}_1$, and $\underline{T}_0$ for each sub-region of the ATS map. As each set of linear functions was chosen such that it forms a convex epigraph when relaxed, we find the value for $\overset{*}{m}{}^\mathrm{tp}_\mathrm{NOx}$ by evaluating all linear functions and taking the maximum. The final simplified ATS map is

$$\overset{*}{m}{}^\mathrm{tp}_\mathrm{NOx} = \begin{cases} \overset{*}{m}{}^\mathrm{eo}_\mathrm{NOx} & \text{if } b_\mathrm{ATS} = 0 \\ \max(\underline{T}_2 \vartheta_\mathrm{ATS} + \underline{T}_1 \overset{*}{m}{}^\mathrm{eo}_\mathrm{NOx} + \underline{T}_0) & \text{if } b_\mathrm{ATS} = 1 \,, \end{cases} \tag{17}$$

where the vectors $\underline{T}$ depend on the ATS integer i_ATS. Figure 3 shows the resulting ATS map with its regions and sub-regions.

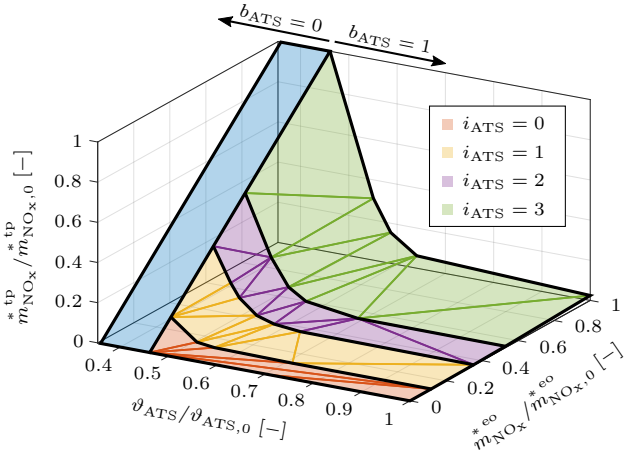

Fig. 3. Region-wise convex adapted look-up map for the chemical ATS model. All values are normalized.

Equation (9) is approximated by

$$\frac{\mathrm{d}m^\mathrm{tp}_{\mathrm{NO_x}}}{\mathrm{d}t} = \overset{*}{m}{}^\mathrm{tp}_{\mathrm{NO_x}}(\vartheta_\mathrm{ATS}, \overset{*}{m}{}^\mathrm{eo}_{\mathrm{NO_x}}) \,. \tag{18}$$

4.2 Resulting MICP

As (12), (13), (15), and (17) describe nonlinear equality constraints of the OCP, they must be relaxed in order to formulate an MICP. During the model formulation, the inequality constraints were formulated such that they always hold as equalities at the optimal solution, i.e., the relaxation does not alter the resulting optimum. In addition to the gearbox integer variable i_gb, the ATS binary b_ATS and the ATS integer i_ATS were introduced and need to be added to the optimization variables of the OCP. The resulting OCP is

$$\underset{P,\, i_\mathrm{gb},\, b_\mathrm{ATS},\, i_\mathrm{ATS}}{\text{minimize}} \quad \int_0^{t_\mathrm{fin}} P_\mathrm{f} \, \mathrm{d}t \tag{19a}$$

subject to

$$\text{Eqs. (1)-(6), (8), (11c)-(11n), and (18)} \tag{19b}$$

$$b_\mathrm{ATS} \in \{0,\ 1\} \tag{19c}$$

$$i_\mathrm{ATS} \in \{0, 1, 2, 3\} \tag{19d}$$

$$P_\mathrm{b} \geq \alpha P^2 + \beta_1 P \tag{19e}$$
$$P_\mathrm{b} \geq \alpha P^2 + \beta_2 P \tag{19f}$$
$$\overset{*}{m}{}^{\mathrm{eo}}_{\mathrm{NOx}} \geq \nu_2 P_\mathrm{f}^2 + \nu_1 P_\mathrm{f} \tag{19g}$$
$$\text{Eq. (20) if } i_\mathrm{gb} = 0 \tag{19h}$$
$$\text{Eq. (21) if } i_\mathrm{gb} > 0 \tag{19i}$$
$$\text{Eq. (22) if } b_\mathrm{ATS} = 0 \tag{19j}$$
$$\text{Eq. (23) if } b_\mathrm{ATS} = 1 \tag{19k}$$

If $i_\mathrm{gb} = 0$, the following constraints are active:

$$P_\mathrm{f} = 0 \tag{20a}$$
$$\overset{*}{H}_\mathrm{ATS} = 0\,. \tag{20b}$$

If $i_\mathrm{gb} > 0$, the following constraints are active:

$$P_\mathrm{f} \geq \kappa_2 P_\mathrm{e,ts}^2 + \kappa_1 P_\mathrm{e,ts} + \kappa_0 \tag{21a}$$
$$\overset{*}{H}_\mathrm{ATS} = \delta_2 \vartheta_\mathrm{ATS} + \delta_1 \cdot (P_\mathrm{f} - P_\mathrm{e,ts}) + \delta_0\,. \tag{21b}$$

If $b_\mathrm{ATS} = 0$, the following constraints are active:

$$\vartheta_\mathrm{ATS} < \vartheta_\mathrm{ATS,thr} \tag{22a}$$
$$\overset{*}{m}{}^{\mathrm{tp}}_{\mathrm{NOx}} = \overset{*}{m}{}^{\mathrm{eo}}_{\mathrm{NOx}}\,. \tag{22b}$$

If $b_\mathrm{ATS} = 1$, the following constraints are active:

$$\vartheta_\mathrm{ATS} \geq \vartheta_\mathrm{ATS,thr} \tag{23a}$$
$$\overset{*}{m}{}^{\mathrm{eo}}_{\mathrm{NOx}} \geq \overset{*}{m}{}^{\mathrm{eo,lb}}_{\mathrm{NOx}} \tag{23b}$$
$$\overset{*}{m}{}^{\mathrm{eo}}_{\mathrm{NOx}} < \overset{*}{m}{}^{\mathrm{eo,ub}}_{\mathrm{NOx}} \tag{23c}$$
$$\underline{\overset{*}{M}}{}^{\mathrm{tp}}_{\mathrm{NOx}} \geq \underline{T}_2 \vartheta_\mathrm{ATS} + \underline{T}_1 \overset{*}{m}{}^{\mathrm{eo}}_{\mathrm{NOx}} + \underline{T}_0\,. \tag{23d}$$

As in (12)-(17), the dependencies on ω_m, ω_e, and i_ATS are not noted explicitly. The constraints (22a) and (23a)-(23c) guarantee that the region of the ATS map corresponding to b_ATS and i_ATS is evaluated. If $b_\mathrm{ATS} = 1$, the limits $\overset{*}{m}{}^{\mathrm{eo,lb}}_{\mathrm{NOx}}$ and $\overset{*}{m}{}^{\mathrm{eo,ub}}_{\mathrm{NOx}}$ denote the i_ATS-dependent lower and upper bound of $\overset{*}{m}{}^{\mathrm{eo}}_{\mathrm{NOx}}$, respectively and the set of relaxed linear constraints on $\overset{*}{m}{}^{\mathrm{tp}}_{\mathrm{NOx}}$ is summarized in the vector $\underline{\overset{*}{M}}{}^{\mathrm{tp}}_{\mathrm{NO_x}}$.

5. ICO ALGORITHM

Mixed-integer optimization problems are notoriously hard to solve due to their combinatorial nature. The iterative convex optimization (ICO) algorithm presented in this work decouples the optimization of the continuous inputs from the optimization of the discrete inputs by applying two optimization methods. By iterating over the two methods, the solution that minimizes the cost of both optimizations is sought. An application of a similar algorithm to a different problem is presented in Nüesch et al. (2014b). An overview of the algorithm is presented in Fig. 4. The individual blocks are outlined in the following.

The iteration index is denoted by j. The vector $\underline{i}$ contains all discrete inputs, whilst the vector $\underline{\lambda}$ contains the costates resulting from the convex optimization.

$$\underline{i} = \begin{bmatrix} i_\mathrm{gb} \\ b_\mathrm{ATS} \\ i_\mathrm{ATS} \end{bmatrix} \qquad \underline{\lambda} = \begin{bmatrix} \lambda_\xi \\ \lambda_\vartheta \\ \lambda_{\mathrm{NO_x}} \end{bmatrix} \tag{24}$$

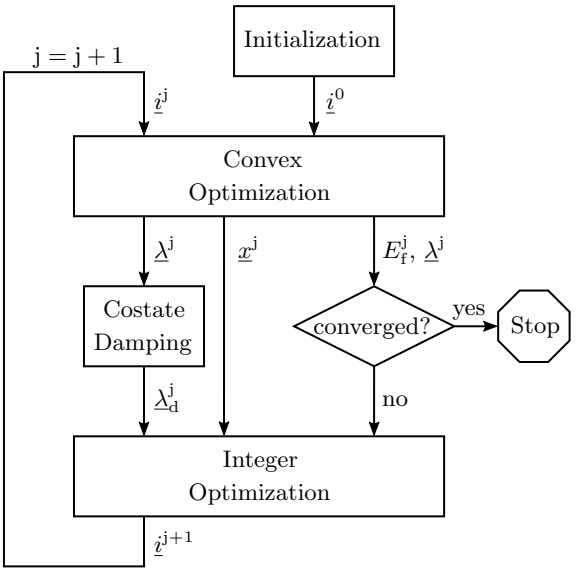

Fig. 4. Overview of the ICO algorithm.

The costate λ_ξ is associated to the state of charge, λ_ϑ is associated to the ATS temperature, and $\lambda_{\mathrm{NO_x}}$ is associated to the accumulated tailpipe $\mathrm{NO_x}$ mass. By evaluating PMP for the MICP we find that the costates λ_ξ and $\lambda_{\mathrm{NO_x}}$ are constant, as the Hamiltonian does not depend on the state of charge or the current tailpipe $\mathrm{NO_x}$ mass flow. The costate λ_ϑ on the other hand, is time-dependent.

5.1 Convex Optimization

The Convex Optimization block solves the OCP stated in (19) for given discrete variables $\underline{i}$ using the parser YALMIP (Lofberg (2004)) and the solver ECOS (Domahidi et al. (2013)). To deal with infeasible problems during intermediate iteration steps, soft constraints are used for the terminal constraints on ξ and $m^{\mathrm{tp}}_{\mathrm{NOx}}$. We add the slack variables $\epsilon_\xi \geq 0$ and $\epsilon_{\mathrm{NO_x}} \geq 0$ to the terminal constraints (11d) and (11h) as

$$\xi(t_\mathrm{fin}) \geq \xi_0 - \epsilon_\xi \tag{25}$$
$$m^{\mathrm{tp}}_{\mathrm{NO_x}}(t_\mathrm{fin}) \leq \overline{m}^{\mathrm{tp}}_{\mathrm{NO_x}} + \epsilon_{\mathrm{NO_x}} \tag{26}$$

and we add the terminal cost

$$w_\xi \epsilon_\xi + w_{\mathrm{NO_x}} \epsilon_{\mathrm{NO_x}} \tag{27}$$

with weights w_ξ and $w_{\mathrm{NO_x}}$ subject to tuning to the objective (19a). To ensure that a non-slacked solution to the OCP is found if it exists, w_ξ and $w_{\mathrm{NO_x}}$ need to be chosen at least as large as the a priori unknown costates λ_ξ and $\lambda_{\mathrm{NO_x}}$. On the other hand, they should be chosen as small as possible to avoid issues with the relaxation of the constraints of the OCP. A reasonable trade-off is to set the weights w to twice the value of the corresponding costates obtained by running an optimization on the legislative cycle. The outputs of the Convex Optimization block are the costates $\underline{\lambda}$, the states $\underline{x}$, and the accumulated fuel energy E_f found by integrating the fuel power P_f over the entire driving mission.

5.2 Integer Optimization

In Ritzmann et al. (2019), we devised an algorithm to rapidly solve the HEV energy management problem for the HEV without accounting for the ATS and the emissions. The OCP was solved efficiently by exploiting the fact that neglecting the state dependency of the Hamiltonian results in a limited loss in accuracy. The dynamic optimization problem was reformulated as a static optimization problem, which is much easier to solve. A similar approach is applied here.

The Hamiltonian resulting from the OCP in (19) has the form

$$H = g(P, i_{\mathrm{gb}}) + \underline{\lambda}^{\intercal} \underline{f}(P, i_{\mathrm{gb}}, \vartheta_{\mathrm{ATS}}) \,, \tag{28}$$

where the stage cost $g(P, i_{\mathrm{gb}})$ corresponds to the fuel power and $\underline{f}(P, i, \vartheta_{\mathrm{ATS}})$ is a vector describing the state dynamics given by (4), (6), and (18). In (28) we notice that the Hamiltonian only depends on the inputs and the ATS temperature. In the Integer Optimization block the value of ϑ_{ATS} is approximated using the temperature $\vartheta_{\mathrm{ATS}}^{\mathrm{j}}$ obtained from the previous evaluation of the Convex Optimization block. The Hamiltonian is approximated as

$$\tilde{H} = P_{\mathrm{f}} + \underline{\lambda}_{\mathrm{d}}^{\mathrm{j}\,\intercal} \begin{bmatrix} -\dfrac{P_{\mathrm{b}}(P)}{Q_{\max} V_{\mathrm{oc}}} \\ \dfrac{1}{m_{\mathrm{ATS}} c_{\mathrm{ATS}}} \cdot \Big(\overset{*}{H}_{\mathrm{ATS}}(P, i_{\mathrm{gb}}, \vartheta_{\mathrm{ATS}}^{\mathrm{j}}) \\ - \alpha_{\mathrm{hl}} S \cdot (\vartheta_{\mathrm{ATS}}^{\mathrm{j}} - \vartheta_{\mathrm{amb}}) \Big) \\ \overset{*}{m}_{\mathrm{NOx}}^{\mathrm{tp}}(\vartheta_{\mathrm{ATS}}^{\mathrm{j}}, P, i_{\mathrm{gb}}) \end{bmatrix}, \tag{29}$$

where $\underline{\lambda}_{\mathrm{d}}^{\mathrm{j}}$ are the damped costates which are introduced in the next section. This approximation results in a static optimization problem, which is solved by evaluating $\tilde{H}$ for a grid consisting of all values for i_{gb} and of quantized values for P and by identifying the minimum for each time instance. This keeps the required computation time for the integer optimization low.

Once the optimal values of i_{gb} and P are found, they are applied in a forward simulation of the thermal ATS model and the resulting temperature trajectory is used to determine b_{ATS}. The discrete variable vector $\underline{i}$ is then passed to the Convex Optimization block.

5.3 Costate Damping

To avoid any oscillations over ICO iterations, the costates resulting from the convex optimization are damped according to

$$\underline{\lambda}_{\mathrm{d}}^{\mathrm{j}} = \begin{cases} \underline{\lambda}^{0} & \text{if } \mathrm{j} = 0 \\ \psi^{\mathrm{j}} \underline{\lambda}^{\mathrm{j}} + (1 - \psi^{\mathrm{j}}) \cdot \underline{\lambda}^{\mathrm{j}-1} & \text{if } \mathrm{j} > 0 \,. \end{cases} \tag{30}$$

Instead of a constant damping factor ψ as in Nüesch et al. (2014b), we heuristically choose ψ^{j} as

$$\psi^{\mathrm{j}} = \max\left(\frac{0.55}{\mathrm{j}}, \, 0.07 \right) \,. \tag{31}$$

Initially, in order to obtain a fast convergence, ψ^{j} is large and the damping is limited. As we iterate, ψ^{j} is decreased to increase damping and avoid any undesired oscillations around the optimum. However, a minimum of 0.07 is always retained.

5.4 Initialization

To initialize the ICO algorithm, the PMP-based method presented in Ritzmann et al. (2019) is used to find the optimal solution of the HEV energy management problem without considering emissions. In addition to the gear selection variable i_{gb}, the corresponding ATS variables b_{ATS} and i_{ATS} are then found through a forward simulation of the engine-out $\mathrm{NO_x}$ model and the thermal ATS model, and the discrete input vector $\underline{i}^{0}$ is passed to the Convex Optimization block.

5.5 Convergence Criterion

To check the convergence of the ICO algorithm, we analyse the accumulated fuel energy E_{f} as well as the non-damped costates λ_{ξ} and $\lambda_{\mathrm{NO_x}}$. The ICO iteration is considered converged and the algorithm is stopped if all the tolerances

$$\left| \frac{E_{\mathrm{f}}^{\mathrm{j}} - E_{\mathrm{f}}^{\mathrm{j}-1}}{E_{\mathrm{f}}^{\mathrm{j}}} \right| \leq 0.001 \tag{32}$$

$$\left| \frac{\lambda_{\xi}^{\mathrm{j}} - \lambda_{\xi}^{\mathrm{j}-1}}{\lambda_{\xi}^{\mathrm{j}}} \right| \leq 0.05 \tag{33}$$

$$\left| \frac{\lambda_{\mathrm{NO_x}}^{\mathrm{j}} - \lambda_{\mathrm{NO_x}}^{\mathrm{j}-1}}{\lambda_{\mathrm{NO_x}}^{\mathrm{j}}} \right| \leq 0.05 \tag{34}$$

are fulfilled and a non-slacked solution is found. By checking E_{f}, we determine whether a further reduction in the fuel consumption is possible. By checking the constant costates λ_{ξ} and $\lambda_{\mathrm{NO_x}}$, we prevent any oscillations in the strategy.

6. RESULTS

To test the performance of the proposed ICO algorithm, we compare it to a DP benchmark. An urban driving mission with a distinct elevation profile is used. The driving mission was obtained using the open-source software Simulation of Urban MObility (SUMO, Behrisch et al. (2011)) and is shown in the upper two plots of Fig. 5. An initial temperature in the range of $\vartheta_{\mathrm{ATS,thr}}$ was chosen such that the ATS is able to reduce $\mathrm{NO_x}$ emissions, and the accuracy of ICO can be assessed by analysing the results. The computation times reported are obtained using a PC with a 2.5 GHz quad-core processor, and 16 GB of RAM.

First, we check the performance of the ICO algorithm itself. To exclude any model mismatch from the analysis, we run both DP and ICO on the simple model presented in Sec. 4.1. The performance comparison of the two methods is shown in Table 1. Both methods meet the state-of-charge and tailpipe $\mathrm{NO_x}$ constraint exactly. As the ICO algorithm does not suffer from a quantization error, it outperforms the DP benchmark and reduces the amount of fuel consumed by 0.24%. We conclude that the ICO algorithm converges to the global optimum. The required calculation time was reduced from one week to just 49 s.

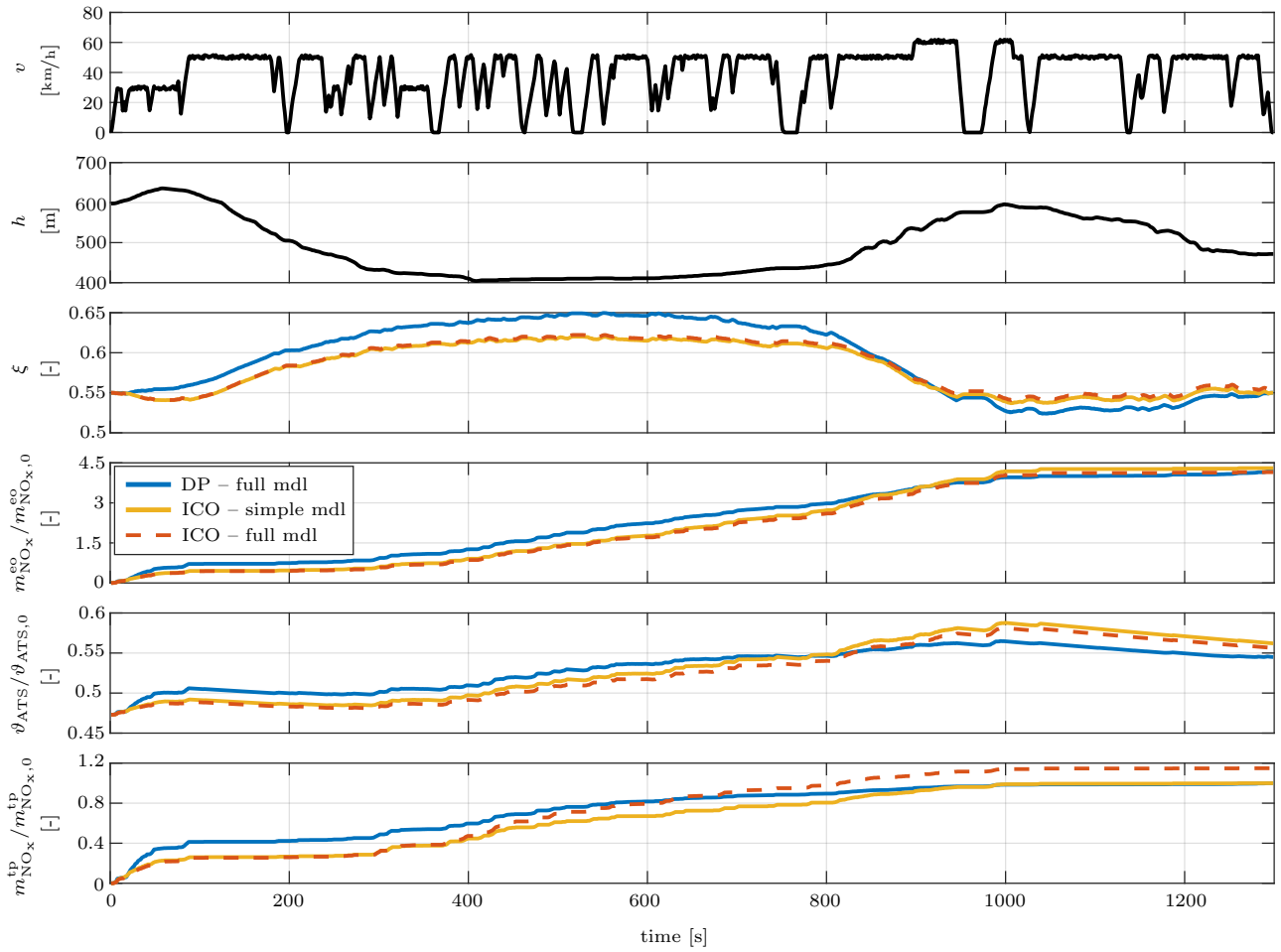

Fig. 5. Optimization result of DP optimization on the full model (blue), of the ICO optimization on the simple model (yellow), and the evaluation of the ICO solution on the full model (dashed red). From the top: vehicle velocity, elevation, state of charge, normalized accumulated mass of engine-out NO_x, normalized ATS temperature, and normalized accumulated tailpipe NO_x mass.

Table 1. Performance on the simple model.

Method	t_{calc}	m_f [%]	ξ [%]	$m^{tp}_{NO_x}$ [%]
DP	1 week	100	100	100
ICO	49 s	99.76	100	100

To analyse the effect of model mismatch on the solution, we run DP on the full model presented in Sec. 1 and compare the result to that obtained by evaluating the ICO solution on the full model. The result is shown in Fig. 5. The performance on the full model is further summarized in Table 2. While the ICO algorithm meets the state-of-charge and tailpipe NO_x constraint exactly for the simple model (yellow curves), an offset results when the ICO solution is evaluated on the full model (dashed red curves). The offset of 0.7% in the fuel consumption and of 0.88% in the state of charge is limited. However, the offset of 14.9% in the accumulated tailpipe NO_x mass is much larger.

We identify the source of this offset by comparing the ICO solution with the ICO solution evaluated on the full model. While the engine-out NO_x mass flow is almost identical, a slight overestimation of the ATS temperature by the simple model is observed. The offset in the accumulated tailpipe NO_x mass is almost exclusively attributed to the operation between 400 s and 800 s. In this section, the ATS operates in the non-convex part of the ATS map, see Fig. 2, where the error introduced by fitting a region-wise convex map is largest. Furthermore, in this part of the ATS map, the tailpipe NO_x mass flow is very sensitive to the ATS temperature and even the small offset in the ATS temperature has a strong effect on the tailpipe NO_x mass flow. The offset in the accumulated tailpipe NO_x mass is caused mainly by the inaccuracy of the region-wise convex ATS map for normalized ATS temperatures between 0.5 and 0.55.

Table 2. Performance on the full model.

Method	t_{calc}	m_f [%]	ξ [%]	$m^{tp}_{NO_x}$ [%]
DP	1 week	100	100	100
ICO	49 s	100.70	100.88	114.90

7. CONCLUSION

In this paper, we identify the optimal energy and emissions management strategies for a HEV by jointly accounting for the battery and the ATS dynamics, achieving a charge-sustaining operation, and keeping the tailpipe NO_x emis-

sions below the legislative limit. By simplifying the vehicle model we were able to formulate the optimal control problem as a mixed-integer convex problem and solve it using the proposed iterative convex optimization (ICO) algorithm. For the simple model, the ICO algorithm was shown to find the globally optimal solution. For the full model, the result obtained using the ICO algorithm shows an offset in the accumulated tailpipe NO_x mass of 14.9%, but manages to capture the qualitative behaviour of the DP benchmark. The calculation time could be reduced from one week for the DP benchmark to just 49 s for the ICO solution.

As the proposed algorithm is designed for online optimal control with feedback, the accuracy of the method is likely sufficient. Its short computation time makes the proposed algorithm real-time capable. Therefore, the ICO algorithm constitutes an efficient optimization method to solve the energy and emissions management problem online even if integer control variables such as gear selection or the engine on/off command have to be optimized. The implementation of an online controller based on the proposed method is the logical next step.

As the current limitation of the ICO algorithm is given by the model mismatch resulting from formulating a convex problem, an optimization algorithm could be considered that is similar to the ICO algorithm, but relies on a continuously differentiable model and a non-convex mixed-integer problem. While the model error would be reduced, it would no longer be possible to formulate an MICP and the global optimality guarantee would be lost. The resulting trade-off between performance and robustness needs to be analysed carefully.

ACKNOWLEDGEMENTS

We thank FPT Motorenforschung AG and the Swiss Federal Office of Energy (SFOE) for supporting this project. We also thank B. Rohrbach for her helpful comments and advice during the proofreading phase.

REFERENCES

Ambühl, D. (2009). *Energy management strategies for hybrid electric vehicles*. Ph.D. thesis, ETH Zürich, Dissertation No. 18435.

Behrisch, M., Bieker, L., Erdmann, J., and Krajzewicz, D. (2011). SUMO–simulation of urban mobility: an overview. In *Proceedings of SIMUL 2011, The Third International Conference on Advances in System Simulation*. ThinkMind.

Bellman, R. (1956). Dynamic programming. Technical report, Rand Corp. Santa Monica CA.

Boltyanski, V.G., Gamkrelidze, R.V., Mishchenko, E.F., and Pontryagin, L.S. (1960). The maximum principle in the theory of optimal processes of control. *IFAC Proceedings Volumes*, 1(1), 464–469.

Domahidi, A., Chu, E., and Boyd, S. (2013). ECOS: An SOCP solver for embedded systems. In *2013 European Control Conference (ECC)*, 3071–3076. IEEE.

Käfer, S. (2004). *Trockenharnstoff-SCR-System und Betriebsstrategie für Fahrzeuge mit Dieselmotor*. Ph.D. thesis, Technische Universität Kaiserslautern.

Kessels, J., Willems, F.P.T., Schoot, W.J., and Van Den Bosch, P.P.J. (2010). Integrated energy & emission management for hybrid electric truck with SCR aftertreatment. In *Vehicle Power and Propulsion Conference (VPPC), 2010 IEEE*, 1–6. IEEE.

Kuchly, J., Nelson-Gruel, D., Charlet, A., Chamaillard, Y., and Nouillant, C. (2019). Projected Gradient and Model Predictive Control: Optimal Energy and Pollutants Management for Hybrid Electric Vehicle. *IFAC-PapersOnLine*, 52(5), 121–127.

Lee, J. and Leyffer, S. (2011). *Mixed integer nonlinear programming*, volume 154. Springer Science & Business Media.

Lofberg, J. (2004). YALMIP : a toolbox for modeling and optimization in MATLAB. In *2004 IEEE International Conference on Robotics and Automation (IEEE Cat. No.04CH37508)*, 284–289. doi: 10.1109/CACSD.2004.1393890.

Ma, Y. and Wang, J. (2017). Integrated power management and aftertreatment system control for hybrid electric vehicles with road grade preview. *IEEE Transactions on Vehicular Technology*, 66(12), 10935–10945.

Nüesch, T., Cerofolini, A., Mancini, G., Cavina, N., Onder, C., and Guzzella, L. (2014a). Equivalent consumption minimization strategy for the control of real driving NOx emissions of a diesel hybrid electric vehicle. *Energies*, 7(5), 3148–3178.

Nüesch, T., Elbert, P., Flankl, M., Onder, C., and Guzzella, L. (2014b). Convex optimization for the energy management of hybrid electric vehicles considering engine start and gearshift costs. *Energies*, 7(2), 834–856.

Ritzmann, J., Christon, A., Salazar, M., and Onder, C. (2019). Fuel-optimal power split and gear selection strategies for a hybrid electric vehicle. Technical report, SAE Technical Paper.

Sciarretta, A. and Guzzella, L. (2007). Control of hybrid electric vehicles. *IEEE Control Systems Magazine*, 27(2), 60–70.

Simon, A., Nelson-Gruel, D., Charlet, A., Jaine, T., Nouillant, C., and Chamaillard, Y. (2018). Optimal supervisory control of a Diesel HEV taking into account both DOC and SCR efficiencies. *IFAC-PapersOnLine*, 51(9), 323–328.

Sundström, O. and Guzzella, L. (2009). A generic dynamic programming Matlab function. In *Control Applications, (CCA) & Intelligent Control, (ISIC), 2009 IEEE*, 1625–1630.

Tschopp, F., Nüesch, T., Wang, M., and Onder, C. (2015). Optimal energy and emission management of a Diesel hybrid electric vehicle equipped with a selective catalytic reduction system. Technical report, SAE Technical Paper.

Zentner, S., Asprion, J., Onder, C., and Guzzella, L. (2014). An equivalent emission minimization strategy for causal optimal control of diesel engines. *Energies*, 7(3), 1230–1250.

Zhao, J. and Wang, J. (2014). Model predictive control of integrated hybrid electric powertrains coupled with aftertreatment systems. In *ASME 2014 Dynamic Systems and Control Conference*. American Society of Mechanical Engineers.